J. Water Environ. Nanotechnol., 7(4): 351-362 Autumn 2022

ORIGINAL RESEARCH PAPER

The influence of Cu doped ZrO_2 catalyst for the modification of the rate of a photoreaction and forming microorganism resistance

R. Jeba[1,4,*], S. Radhika[2,4], CM. Padma[3,4], X. Ascar Davix[5]

[1] *Research Scholar, Reg.No:18223282132002, Women's Christian College, Tamilnadu, India-629001*
[2] *Department of Physics, Pioneer Kumaraswamy College, Tamilnadu, India- 629003*
[3] *Department of Physics, Women's Christian College, Tamilnadu, India-629001*
[4] *Affiliated to Manonmaniam Sundaranar University, Abishekapatti, Tirunelveli, India- 627012*
[5] *Department of Electronics and Communication Engineering, R.V.R. & J.C. College of Engineering, Andhra,Pradesh, India - 522019*

Received: 2022-07-18 Accepted: 2022-09-07 Published: 2022-10-01

ABSTRACT

Pure and copper-doped Zirconium oxide nanoparticles were synthesized using a co-precipitation process and investigated the effect of doping on photocatalytic and anti-microbial activities. The prepared samples are pure tetragonal phase, as shown by the X-ray diffraction pattern, and the crystallite size decreases as the dopant concentration increases. Higher dopant concentrations resulted in needle-shaped morphology, as seen in the SEM image. The presence of Zr, Cu, and O in the sample is confirmed by EDS analysis. According to UV-VIS analysis, when the Cu content is increased, a more significant wavelength absorption band edge is formed, and the band gap reduces with the increase in dopant concentration. All samples have magnetic hysteresis loops with diamagnetic background effects, according to VSM tests. A prominent and influential peak at 485nm in the PL spectra suggests that ZrO_2 nanoparticles emit blue light. The produced nanoparticles were utilized as a photocatalyst to degrade Methylene Blue (MB) dye, and the results indicate that a high dopant concentration (0.08wt percent) outperforms pure and other dopant concentrations. Copper-doped ZrO_2 has moderate anti-bacterial and anti-fungal activities.

Keywords: *Co-precipitation, Cu-doped ZrO_2, photocatalysis, anti-microbial.*

How to cite this article
Jeba R., Radhika S., Padma C M., Ascar Davix X. The influence of Cu doped ZrO_2 catalyst for the modification of the rate of a photoreaction and forming microorganism resistance. J. Water Environ. Nanotechnol., 2022; 7(4): 351-362.
DOI: 10.22090/jwent.2022.04.002

INTRODUCTION

Zirconium dioxide (ZrO_2), often known as Zirconia, is a ceramic oxide frequently used in dental bridges and crowns, diamond stimulants, oxygen sensors, fuel cell membranes, and paint additives. Many researchers have prioritized the Zirconia study because due to its chemical and physical features, including phase stability, hardness, high melting point, high refraction indices, and microbial resistance [1]. At high temperatures, Zirconia can allow oxygen ions to travel through the particle structure freely. Monoclinic Zirconia has a temperature less than 1170° C, tetragonal Zirconia has a temperature of 1170° C to 2370° C, and the cubic form of Zirconia has a temperature greater than 2370° C. With the increase in temperature, a phase change occurs, resulting in enormous strains. The thermal, mechanical, and electrical properties of metals such as Zn, CO, Cu, Mg, Ce, Ni, and Fe are improved by doping. The bandgap of ZrO_2 varies depending on the phase and the manner of synthesis. Metal doping in Zirconia is predicted to enhance its properties and uses [2].

Compared to other metal oxides, Zirconia is a stable metal oxide over an extensive pH range [11,12]. According to the literature, few studies have been carried out on Cu-doped Zirconia that

* Corresponding Author Email: *jeba170787@gmail.com*

was synthesized by the Sol-gel process, and the structural and optical properties were examined [1]. The manufacture of Zirconium Oxide nanoparticles is done in a variety of ways. The Co-precipitation method is employed to prepare Cu-doped Zirconia nanoparticles in this study. For the creation of nanoparticles, the co-precipitation approach is straightforward and effective [16-19]. The transfer of holes from the valance band to the surface produces an oxidative hydroxyl radical, which induces efficient MO degradation [3]. Thermal treatment was used to modify the hydroxyl groups on the photocatalyst's surface to improve degrading efficiency [4]. Due to the wide bandgap and many polymorphs, the photocatalytic activity of Zirconia nanoparticles is limited [5]. The photocatalytic activity of Cu-doped ZrO_2 nanoparticles was investigated against Methyl Orange (MO) dye using a hydrothermal technique [3].

Nanostructured materials could also be used in biomedical applications. In this study, we investigated the anti-microbial activity of Zirconia nanoparticles in addition to their photocatalytic activity. Many studies on metal oxide nanoparticles such as TiO2, MgO, ZnO, and ZrO_2 for anti-microbial activity have been conducted [13-15]. The anti-microbial activity of Cu-doped Zirconia nanoparticles is examined in this paper.

EXPERIMENTAL TECHNIQUE

Pure and Cu-Doped ZrO_2 Nanoparticles by Co-precipitation method

NaOH as a precipitating agent, pure and Cu-doped zirconium oxide nanoparticles was synthesized. The ratio of Zirconium oxychloride to sodium hydroxide in an aqueous solution was 0.5:2. Drops of NaOH solution were added until the pH reached 12, and the mixture was agitated repeatedly for 2 hours at 60°C. Finally, to remove contaminants, the resulting precipitate slurry was filtered and washed with distilled water several times before being rinsed with acetone. After drying, the residue was crushed into a fine powder using a mortar and pestle. The resulting ZrO_2 was then annealed for 2 hours at 500°C. Following that, Cu-doped ZrO_2 nanoparticles for 0.04, 0.08, and 0.12wt percent strontium concentrations were synthesized using the same process; the resulting products are referred to as Cu-1, Cu-2, and Cu-3, respectively.

Photocatalytic activity test

On the degradation of methylene blue (MB), the photocatalytic activity of pure and Cu-doped ZrO_2 was investigated. A 0.1M, 50ml aqueous solution of methylene blue was prepared, and 0.2g of photocatalyst (Cu-1, Cu-2, and Cu-3) was suspended in it. The experiment was carried out in the presence of UV light. The solution is continuously stirred while being exposed to a 50W halogen lamp. Every 60 minutes, 4ml of dye solution was removed from the system, and the dye removal efficiency was determined using a UV-Vis spectrometer.

Kirby-Bauer test (KB test)

The KB test, also known as the disc-diffusion antibiotic sensitivity test, is used for the bacterial inhibition experiment. For the development of bacteria, nutrient agar media with a pH of 7.2 was created and inoculated with the experimenting organism. The complete area of antibiotic discs was sprayed with a suspension of gram-positive and gram-negative bacteria. The reference antibiotic is amikacin, which is also spread alongside the disc. The plate was then incubated for 16 hours at 35°C [20]. In and around the sample, bacterial inhibition zones formed. The diameter of the inhibitory zones was measured after incubation. The agar diffusion method tested the antifungal activity of synthesized materials against *Candida Albicans* and *Candida parapsilosis* fungal strains. Nystatin was employed as a reference antifungal. The zone of inhibition is the area where bacterial growth is stopped due to the compound's bacteriostatic activity, and it is used to measure the compound's inhibitory impact on a specific microorganism [13].

Characterization

The structural properties of synthesized nano zirconia, such as crystallite size and phase identification, were validated using an XPERT-PRO diffractometer in the 10o to 80o diffraction angle 2 range. Using a Perkin Elmer Lambda 35 spectrophotometer, UV VIS spectrums for nano ZrO2 were acquired in the wavelength range of 100 to 1100nm. Scanning electron microscope (SEM) and Energy dispersed X-Ray (EDX) with EV018(CARL ZEISS) and Quantax 200 with X Flash 6130 were used to observe the structural morphology and chemical condition. The magnetic characteristics of the produced nanoparticles

are studied using Lakeshore Vibrating Sample Magnetometer (VSM) measurements.

RESULTS AND DISCUSSION

XRD analysis

Fig. 1 shows the XRD patterns of pure and copper-doped zirconium oxide nanoparticles. The presence of sharp, well-defined peaks shows that the processed samples are extremely crystalline. The peaks at 2 30.24°, 34.97°, 35.31°, 50.59°, 59.92°, 63.04°, and 74.34°, which correspond to planes (011), (002), (110), (112), (013), (202), (220), respectively, are in good agreement with JCPDS card No.50-1089 and confirm the pure tetragonal structure of produced ZrO_2 nanoparticles; no import Cu atoms were successfully integrated into the ZrO_2 lattice following doping, demonstrating that the initial phase was not altered. It has been discovered that there is a minor peak movement towards higher 2 values, which is growing as the copper concentration rises. Because Cu^{2+} has a smaller ionic radius (0.72) than Zr^{4+} (0.80), Cu ions occupy substitution and interstitial lattice positions [1].

Lattice defects such as oxygen vacancies and imperfections are formed in the crystal during doping [2]. The defects produced in the Cu-doped ZrO_2 nanoparticles are analyzed from the XRD pattern in terms of structural and geometrical parameters such as lattice constants, dislocation density, microstrain, and stacking fault. The dislocation density (δ) is the length of dislocation per unit volume which depends on the crystallite size (D) and is calculated using the relation: $=\frac{1}{D^2}$. The stacking fault probability is calculated using the formula $F = \frac{2\pi^2}{45\sqrt{3}\tan\theta}$. The microstrain produced due to the dislocations in the nanoparticles is calculated using the relation, $\text{å} = \frac{\beta\cos\theta}{4}$, where β is the FWHM and θ is the diffraction angle. The calculated values are tabulated in Table 1. The average crystallite size is calculated using the debye Sherrer equation: $D = \frac{0.9\lambda}{\beta\cos\theta}$. It is observed that crystallite size decreases with the increase in dopant concentration. Due to the difference in atomic radii

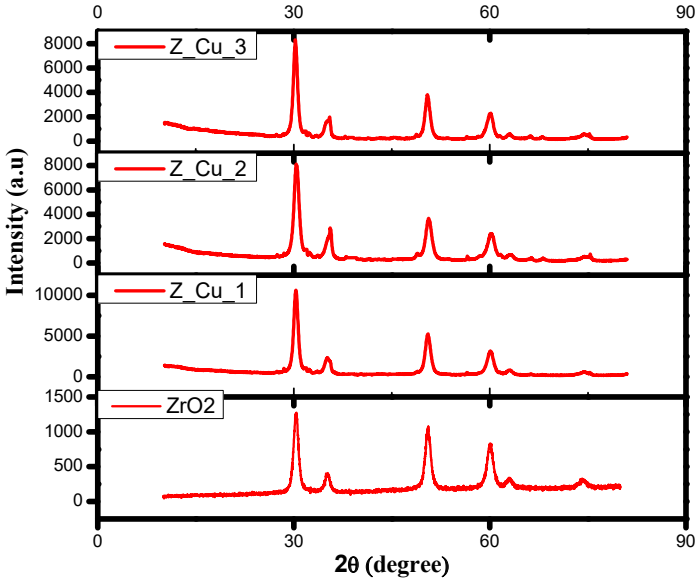

Fig. 1. XRD pattern of pure and copper doped zirconium oxide nanoparticles

Table 1. Lattice and geometrical parameters of pure and Cu doped ZrO_2

Sample detail	Lattice parameters				Geometrical parameters			
	a=b(Å)	c(Å)	Aspect ratio 'c/a'	Unit cell volume 'V' (Å)3	Crystallite Size, D (nm)	Micro strain 'ε' (×10−3)	Dislocation density'δ' (×10^{15} n/m2)	Stacking fault
Pure	3.59	5.27	1.47	58.82	29.74	1.26	1.23	0.48
Cu-1	3.62	5.01	1.40	56.86	10.49	1.43	8.1	0.93
Cu-2	3.62	5.27	1.46	59.81	9.11	1.88	1.6	0.94
Cu-3	3.61	5.08	1.41	57.33	7.88	3.27	2.7	0.93

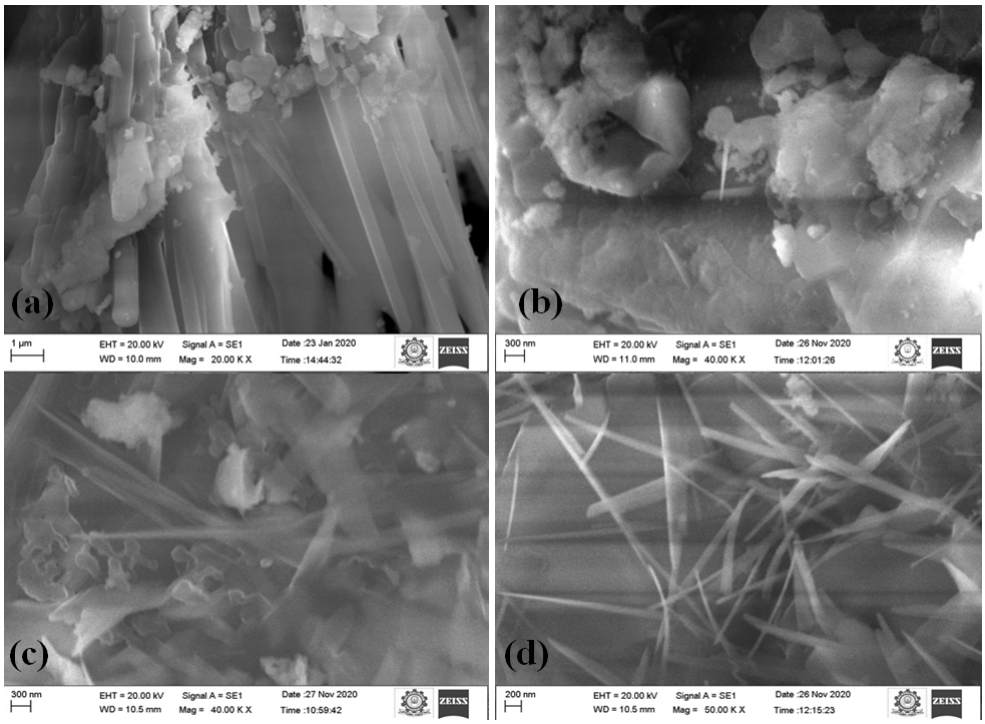

Fig. 2. SEM images of (a) pure (b) Cu-1 (c) Cu-2 (d) Cu-3

of $Cu^{2+}$and Zr^{4+}, there may be the creation of stress in the crystal lattice that leads to low crystallite size, and also the partitioning of copper atoms in the grain boundaries may interrupt the long-range crystallographic ordering that causes the decrease in the crystallite size [3]. For the tetragonal phase, the lattice constants a and c are calculated by using the relation $\frac{1}{d2}=\frac{h2+k2}{a2}+\frac{l2}{c2}$. The calculated values of lattice constants a and c are in good agreement with the reported values [3]. It is noted that for pure and Cu-doped samples the aspect ratio 'c/a' is almost constant which indicates the copper atoms successfully incorporated into the ZrO_2 crystal lattice without modifying its original phase. The volume of ZrO_2 and ZrO_2-Cu unit cell 'V' is calculated by using the relation [4]: $V=\frac{\sqrt{3}a2c}{2}$. The calculated unit cell volume is listed in Table 1.

SEM and EDX analysis

The effect of Cu doping on the morphology of ZrO_2 nanoparticles is investigated by scanning electron microscope (SEM). The micrographs of undoped and copper-doped ZrO_2 nanoparticles under various concentrations are shown in Fig. 2. Rod-shaped morphology was noticed for pure ZrO_2 nanoparticles. For Cu-1 non-homogenous microcrystals without agglomeration is obtained and Cu-2 and Cu-3 needle-shaped morphology was obtained. It was confirmed that from Fig. 2 the Cu^{2+} ions are occupying the interstitial spaces since the orientation of undoped and Cu-doped nanoparticles are different. During doping it is impossible to replace Zr^{4+} ions with Cu^{2+} owing to the smallest ionic radius of copper compared to Zr^{4+}, thus it occupies the interstitial lattice sites and produces defects in ZrO_2 and so it decreases the crystallite size from 29.74nm to 7.88nm. There is a strong effect on the morphology and crystallinity of ZrO_2 while doping Cu in ZrO_2. The Cu-doped ZrO_2 nanoparticles play an important role to change their optical, magnetic, thermal, and biological properties because of the modification of structural and morphological properties. The corresponding EDS spectra of undoped and copper-doped ZrO_2 nanoparticles are shown in Fig. 3 which confirms the presence of Cu, Zr, and O elements in the prepared samples.

UV–vis analysis

UV–Vis absorption spectra of pure and Cu-doped ZrO_2 nanoparticles are shown in Fig. 4. Because of the negatively charged electron

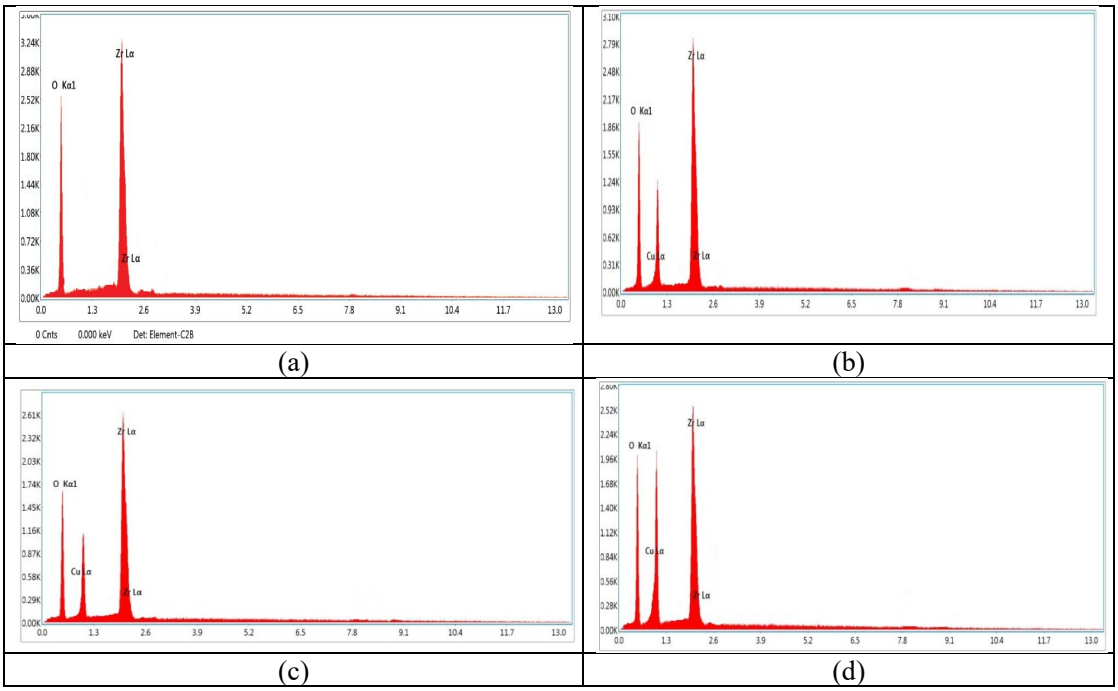

Fig. 3. EDS spectra of (a) pure (b) Cu-1 (c) Cu-2 and (d) Cu-3 ZrO_2 nanoparticles

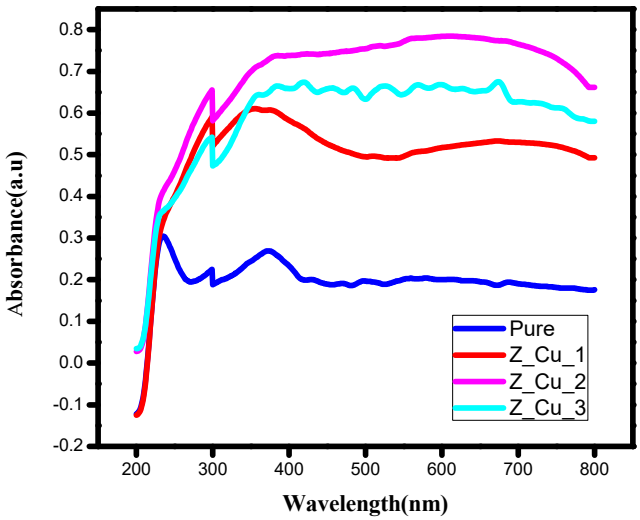

Fig. 4. UV - vis absorbance spectrum

transition from the valence band to the conduction band UV- region peak is obtained. The absorption peak was occurring at 278.6nm for the un-doped sample.

It was observed that a higher wavelength absorption band edge is obtained for doped ZrO_2 nanoparticles and the absorption peak was at 370.25nm for Cu-1, 380.15nm for Cu-2, and 390.05 for Cu-3 respectively. This variation in the absorption band edge leads reduction in the optical band gap energy. The band gap energy was calculated using tauc relation,

$$(\alpha h\vartheta)^n = A(h\vartheta - E_g) \quad (1)$$

Where, $h\vartheta$ is the energy of a photon, E_g is the band gap energy, A is the proportionality constant, and n takes the value $1/2$ for direct allowed transitions and α is the absorption coefficient. The absorption coefficient α is determined using the formula,

$$\alpha = \frac{2.303 \log\left(\frac{1}{T}\right)}{t} \quad (2)$$

Here, 'T' represents transmittance and 't' represents the thickness of the sample. The Tauc plot is drawn and extrapolating the line to the x-axis energy gap is obtained and is shown in Fig. 5. The energy gap values of pure and Cu-1, Cu-2, and Cu-3 doped ZrO_2 are 4.7, 2.5, 1.7, and 1.5 eV.

The optical analysis stipulates the energy gap values were reduced from 4.7eV to 1.5eV with increasing Cu content. This reduction may be due to the use of Cu, a semiconductor with a lower band gap than ZrO_2. Also due to the d-d transition ($2T_{2g} \rightarrow 2A_{2g}$ or $2T_{1g}$), the energy gap is reduced. Because of free charge carriers and many-body interactions, Cu ions manifest charge transfer into various ionic states of the ZrO_2 lattice [5].

Photoluminescence analysis

To study the emission properties of undoped and Cu-doped ZrO_2 nanoparticles photoluminescence spectra were taken with an excitation wavelength of 270 nm. To evaluate the effectiveness of electron-hole trapping and perceived the fact of charge carrier recombination in semiconductors photoluminescence spectra have been used. Fig. 6 shows the emission spectra of prepared samples with various dopant concentrations.

As seen from fig the PL spectra of pure ZrO_2 exhibit peaks at 367,419,485 and 542 nm. Among all these peaks weak peaks at 367 and 419nm indicated UV emission of pure ZrO_2 nanoparticles and the sharp and highly intense peak was occurring at 485nm and a relatively weak peak at 542 indicated blue and green emission of ZrO_2 nanoparticles. Fig shows PL spectra of Cu-doped ZrO_2 nanoparticles that exhibit the same peaks at 367,419,485 and 542nm with reduced intensity while comparing to that of pure ZrO_2 nanoparticles. Owing to the presence of empty oxygen sites in ZrO_2 nanoparticles these emission peaks were thus obtained. Due to the charge transition between the Zr^{4+} conduction band and O^{2-} valance band and also surface defects leads to the n hopping mechanism of electrons [6].

Magnetic Properties

The magnetic properties of pure and Cu-doped ZrO_2 nanoparticles were analyzed using Vibrating Sample Magnetometer (VSM) at room temperature with a maximum field of 15000 Oe. Fig. 7 shows the magnetic hysteresis curve of pure and Cu-doped ZrO_2 nanoparticles. All samples show magnetic hysteresis loops. The saturation magnetization(M_s) of the undoped sample is 586.89 × 10^{-6} emu/gm, for Cu-1 477.03× 10^{-6} emu/gm, Cu-2 488.56× 10^{-6} emu/gm, and Cu-3 456.24× 10^{-6} emu/gm.

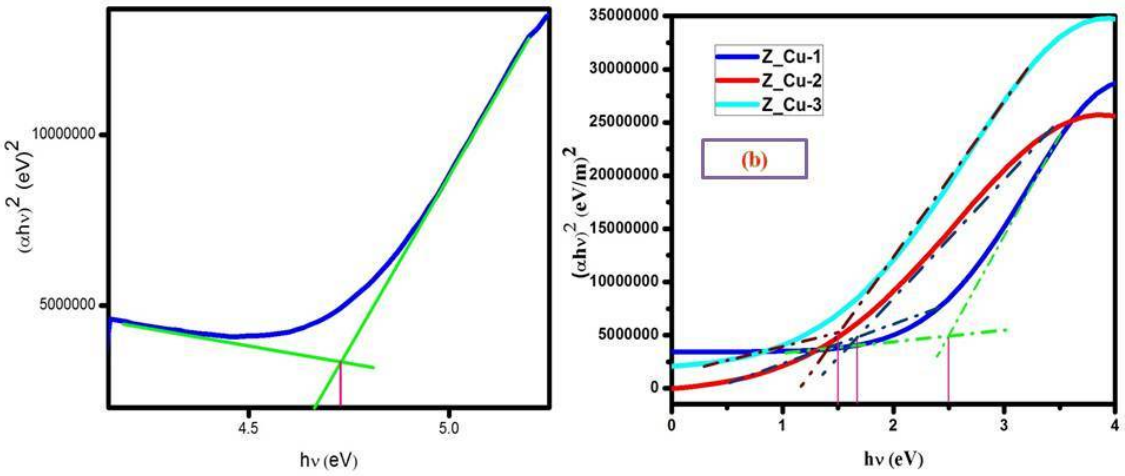

Fig. 5. Tauc plots for (a) pure and (b) Cu doped ZrO_2

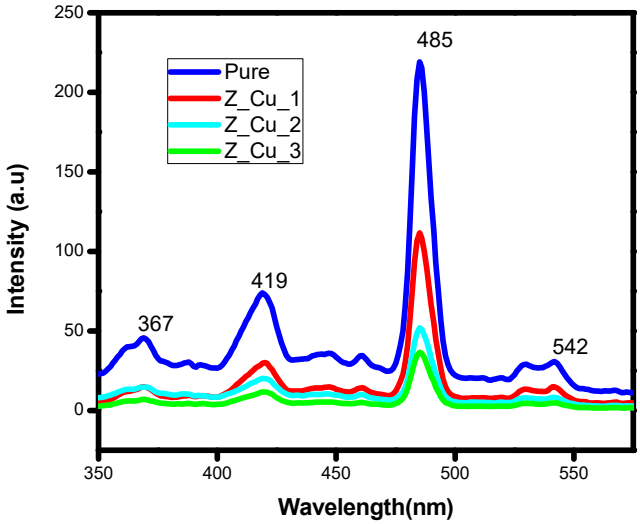

Fig. 6. PL spectra of pure and Cu doped ZrO_2 nanoparticles

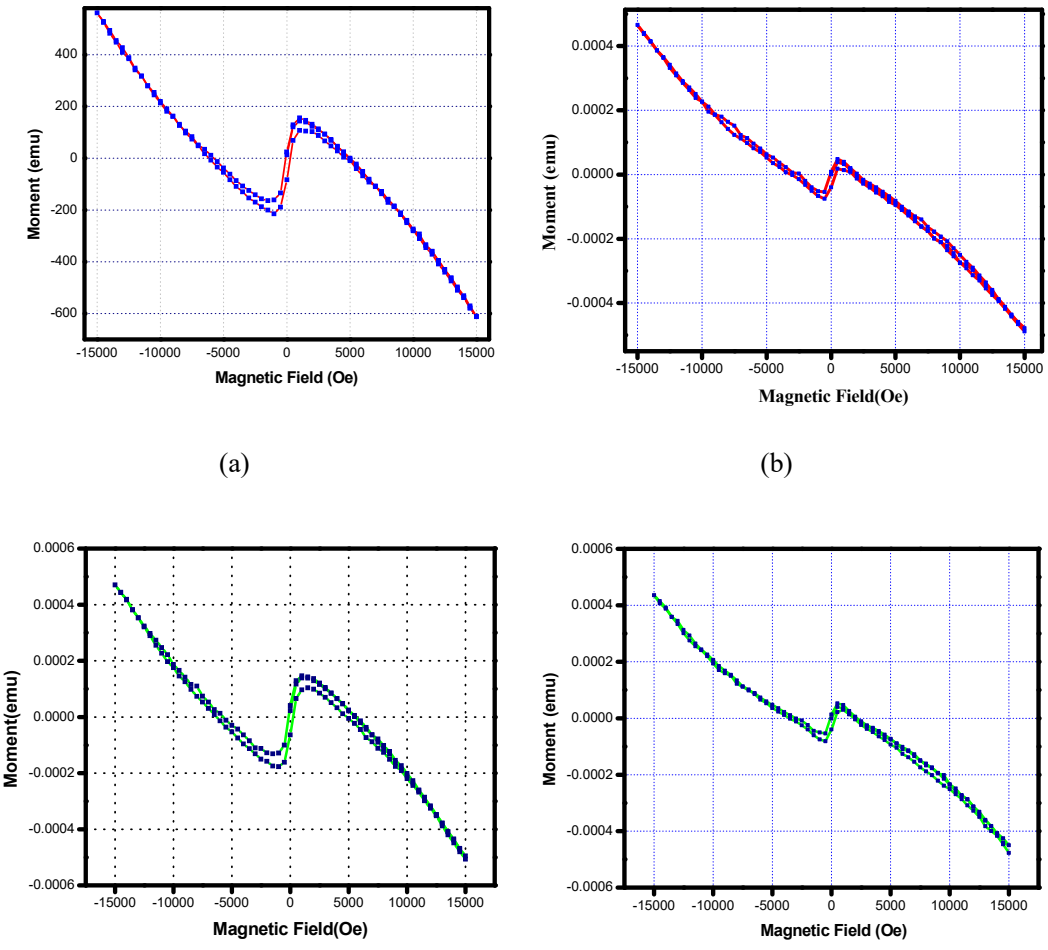

Fig. 7. M-H loops of (a) pure (b) Cu-1 (c) Cu-2 and (d) Cu-3 ZrO_2 nanoparticles

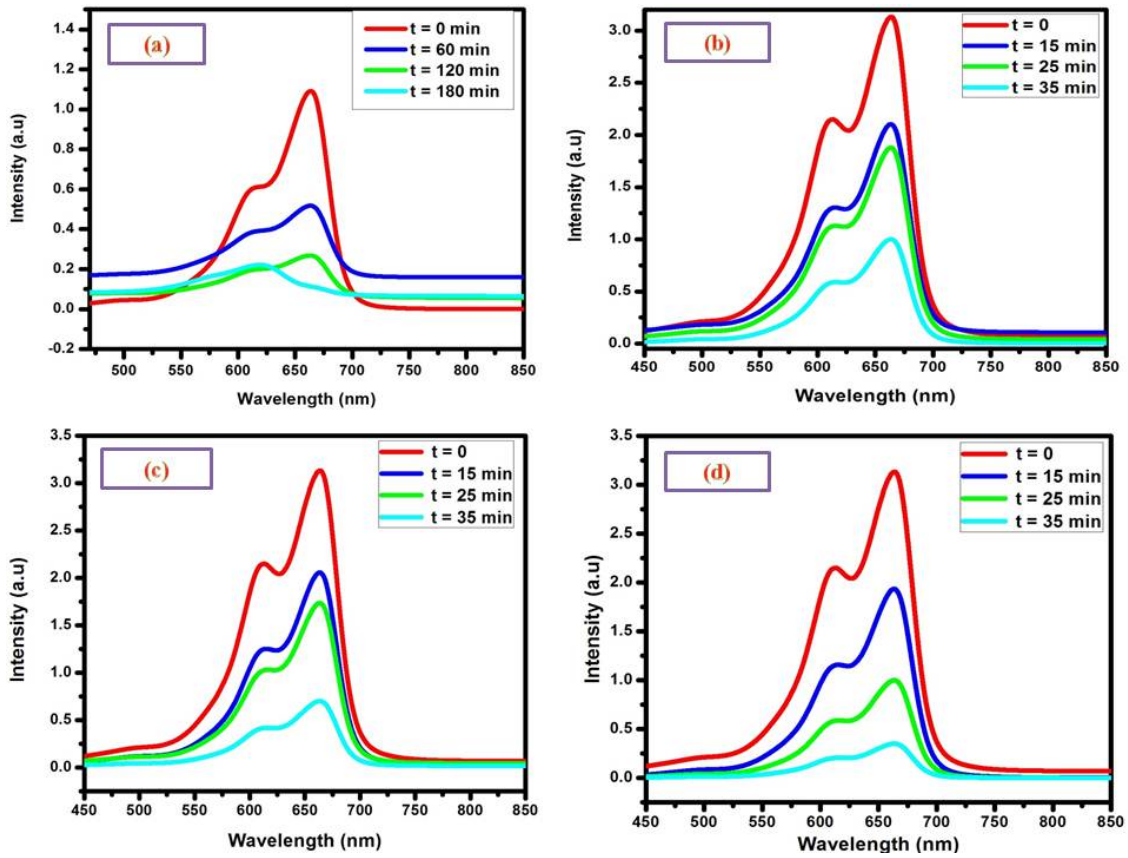

Fig. 8. Absorption spectra of MB solution after degradation by (a) pure ZrO_2 (b) Cu-1 (c) Cu-2 (d) Cu-3

When dopant concentration increases saturation magnetization decreases.

Photo catalytic performance

The photocatalytic performance of prepared samples has been tested for degradation of methylene blue dye under UV irradiation. Due to the increase in the energy gap of solar light, it is not suitable as a source of photocatalysis, since it is a continuous spectrum certain part of spectra is not used for photoelectron hole production. The input energy provided by UV light is large when compared to solar light thus it is sufficient for band gap excitation of electrons in the photocatalysts. The surface composition of ZrO_2 has a great role in the adsorption of dye to enhance photocatalytic activity [12]. Also, various properties of ZrO_2 polymorphs have a great effect on the adsorption and reaction of dyes.

The optical absorption spectra of the degradation of methylene blue (MB) dye using undoped and Cu-doped (Cu-1, Cu-2, and Cu-3) ZrO_2 nanoparticles are shown in Fig. 8. The strong absorption peak of MB arises at 665nm which is due to the chromophore group. The intensity peak of MB at 665 nm was reduced while increasing the irradiation time. It is because of fragmenting of chromophores in the dye throughout the photocatalytic oxidation The following equation provides the removal efficiency (E) of MB degradation,

$$E = \frac{C_0 - C}{C_0} \times 100 \quad \%$$

Where, C_0 is the initial concentration of dye and C is the concentration of MB after UV irradiation. It was observed that Cu-doped ZrO_2 nanoparticles provide faster degradation of MB dye compared to pure ZrO_2. 0.12wt% Cu-3) of Cu doped ZrO_2 provides 89% degradation within 35 minutes, 0.08wt% (Cu-2) provides 78% and

0.04wt% (Cu-1) provides 68% within 35 minutes. The normalized residual concentration of MB dye is estimated using

$$C_t / C_o = A_t / A_o$$

Where C_o and C_t are the initial and residual concentration of MB dye, A_t and A_o are the absorbance intensity at time t and at time t = 0 obtained from the UV-absorbance spectrum [7] and is shown in Fig. 9. The surface area of the prepared sample is high due to the low crystallite size (7.88nm) for Cu-3 as compared to other doping concentrations (Cu-1 and Cu-2). The high surface area provides more active sites for the reaction of photodegradation [8]. Thus copper ions can act as recombination centers and cover the active sites in the host lattice and so it enhances the photocatalytic activity as compared to pure ZrO_2 [9-11]. Due to the morphological change and reduction of crystallite size while doping by Cu ions it enhances photocatalytic activity. Table 1 shows that microstrain increases while crystallite size decreases. The calculated microstrain increases as the Cu content increases from 0.04 to 0.12 wt%, owing to the introduction of more oxygen vacancies. As a result, because Cu-doped ZrO_2 has more oxygen vacancies, it may have higher photocatalytic efficiency [20]. From the observed values of dislocation density, it may be a surface dislocation due to the e atoms on the surface adjusting their positions to accommodate for the absence of neighboring atoms outside the surface [21]. From the outcome of the results, it shows the copper doped (Cu-1, Cu-2and Cu-3) ZrO_2 can effectively enrich the photocatalytic activity

Anti-microbial assessment of pure and Cu-doped ZrO_2 nanoparticles

The synthesized nanoparticles were screened for antibacterial activity against gram-positive pathogens such as Bacillus cereus and Staph aureus and gram-negative pathogen including *E. coli* and *Pseudomonas aeruginosa*. Disc-diffusion antibiotic sensitivity test is used to evaluate their anti-bacterial activity. Nano-scaled particles possess enhanced anti-microbial activity as compared to their bulk part due to their larger surface-to-volume ratio. Pure ZrO_2 exhibit a larger zone of inhibition around 28mm against gram-positive pathogen namely staph aureus compared to other bacteria. Cu-doped ZrO_2 nanoparticles exhibit a higher zone of inhibition against both gram-positive and negative bacteria. The measured values of the inhibition zone in terms of mm are presented in Tables 2 and 3. Fig. 11, clearly shows the synthesized Cu-doped ZrO2 samples have more activity against Bacillus cereus and Staph aureus bacterial strains.

Also, the synthesized samples tested for anti-fungal strains such as *candida Albicans* and *candida parapsilosis*. Figs. 10 and 11 show the inhibition zone of pure and Cu-doped ZrO_2 nanoparticles. Cu-3 sample shows more activity against *Candida parapsilosis* on comparing to other fungal strains. The zone of inhibition for all the samples is presented in Tables 2 and 3. The inhibition zone

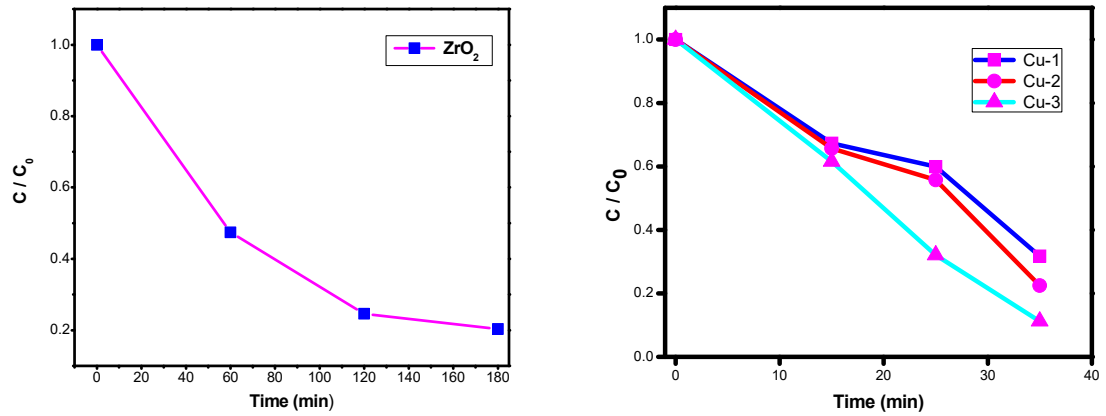

(a) (b)

Fig. 9. MB degradation efficiency of (a) pure and (b) Cu doped ZrO_2

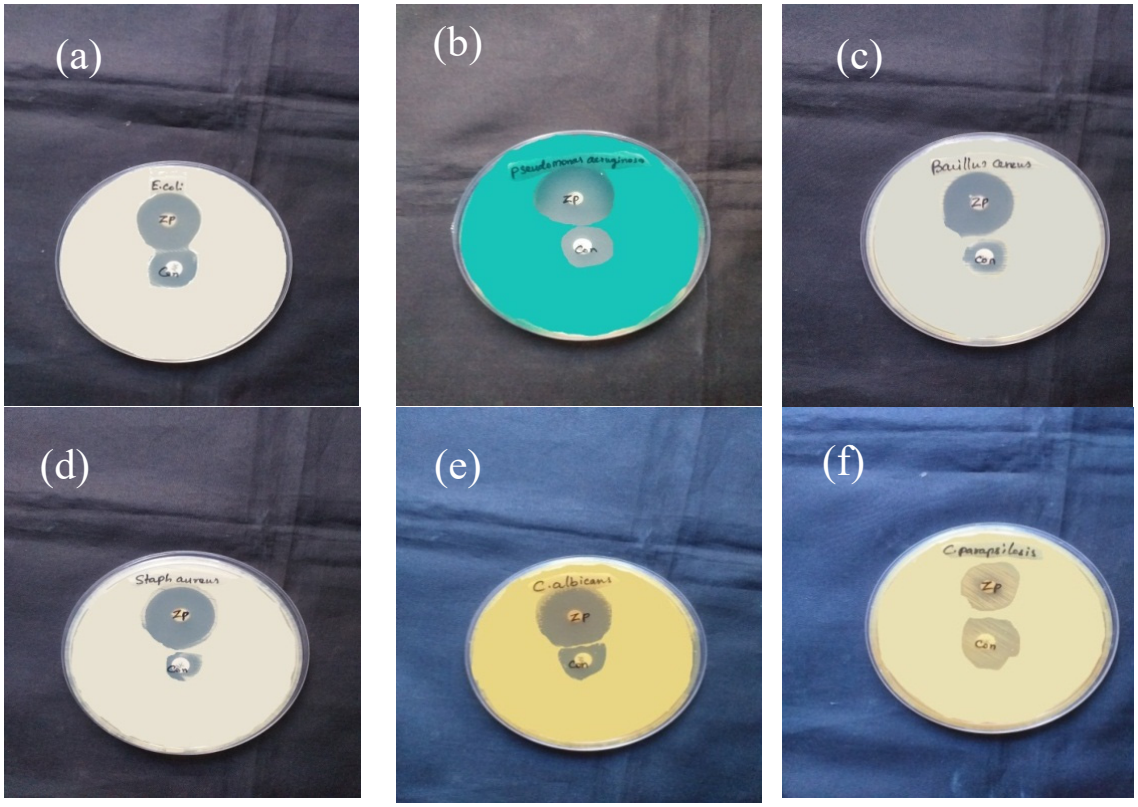

Fig. 10. Anti-bacterial and Anti-fungal effect of pure ZrO_2 nanoparticles

Table 2. Anti-bacterial and Anti-fungal assessment of ZrO_2

Sample	Anti-bacterial Assessment				Antifungal assessment	
	Gram Positive		Gram Negative			
	Bacillus cereus (mm)	Staph aureus (mm)	Escherichia coli (mm)	Pseudomonas aeruginosa (mm)	Candida albicans (mm)	Candida parapsilosis (mm)
Amikacin	16	15	21	37	NA	NA
t-ZrO_2	27	28	26	28	25	18
Nystatin	NA	NA	NA	NA	20	15

Table 3. Anti-bacterial and Anti-fungal assessment of Cu doped ZrO_2

Sample	Anti-bacterial Assessment				Antifungal assessment	
	Gram Positive		Gram Negative			
	Bacillus Subtilis (mm)	Staph aureus (mm)	Escherichia coli (mm)	Pseudomonas aeruginosa (mm)	Candida albicans (mm)	Candida parapsilosis (mm)
Amikacin	27	24	26	21	NA	NA
Cu-1	22	25	17	16	16	18
Cu-2	25	26	18	15	15	22
Cu-3	21	20	20	18	19	23
Nystatin	NA	NA	NA	NA	27	20

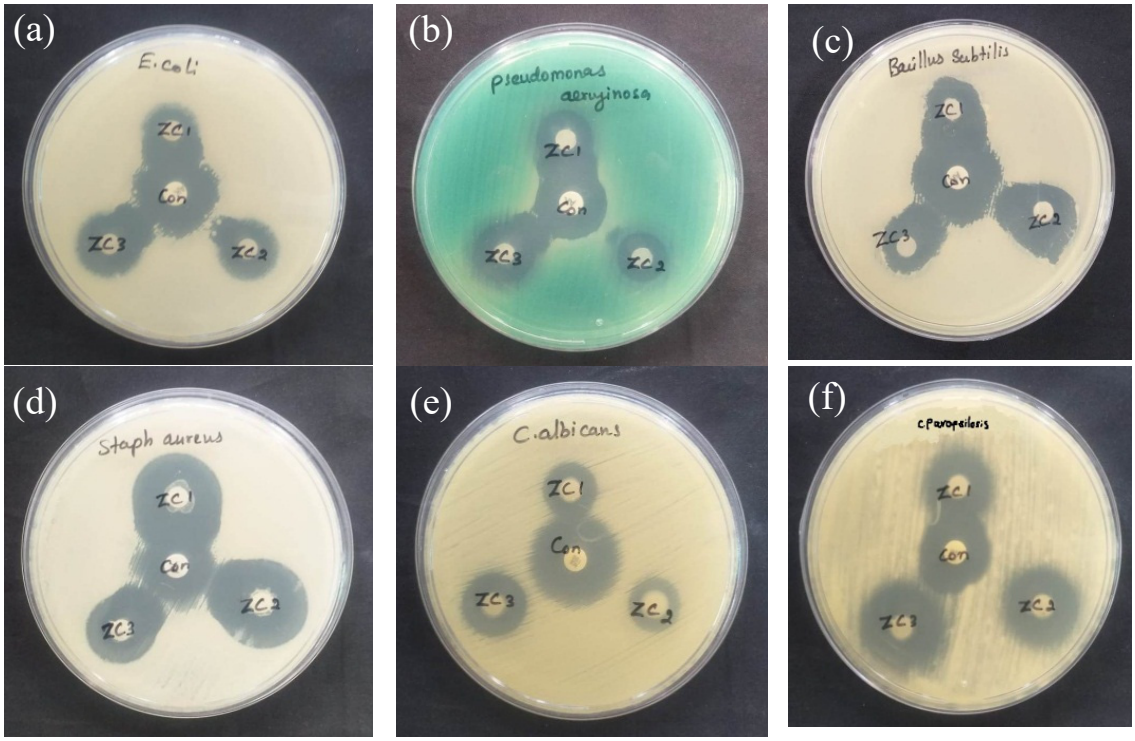

Fig. 11. Anti-bacterial and Anti-fungal effect of Cu doped ZrO_2 nanoparticles

of samples is compared with the control amikacin for bacterial strain and nystatin for fungal strain. A better zone of inhibition is obtained. From this result, we conclude that both pure and Cu-doped ZrO_2 nanoparticles act as good anti-microbial agents.

CONCLUSION

Pure and Cu-doped ZrO_2 nanoparticles were successfully prepared by the Co-precipitation technique and the structural, morphological, optical, magnetic, photocatalytic, and antimicrobial properties were investigated. XRD pattern shows prepared samples show tetragonal crystal structure. SEM analysis revealed that surface properties depend on the doping concentration of Cu. Optical band gaps are found to be decreasing with increasing dopant concentration. PL analysis showed that blue emission of prepared materials. From the photocatalytic results, it was concluded that 89% of methylene blue dye degradation within 35 minutes was observed for high dopant concentration as compared to pure and other dopant concentrations. Copper-doped ZrO_2 has moderate anti-bacterial and anti-fungal activities.

CONFLICT OF INTEREST

On behalf of all authors, the corresponding author states that there is no conflict of interest.

REFERENCES

1. Arjun, A., Dharr, A., Raguram, T. et al. Study of Copper Doped Zirconium Dioxide Nanoparticles Synthesized via Sol-Gel Technique for Photocatalytic Applications. J Inorg Organomet Polym 30, 4989-4998 (2020). https://doi.org/10.1007/s10904-020-01616-4
2. T Mary Jeeva et al 2019 Mater. Res. Express 6 105803. https://doi.org/10.1088/2053-1591/ab42a2
3. Ch Venkata Reddy, I. Neelakanta Reddy, K. Ravindranadh, Kakarla Raghava Reddy, Nagaraj P. Shetti, D. Kim, J. Shim, Tejraj M. Aminabhavi, Copper-doped ZrO2 nanoparticles as high-performance catalysts for efficient removal of toxic organic pollutants and stable solar water oxidation, Journal of Environmental Management, Volume 260, 2020, 110088. https://doi.org/10.1016/j.jenvman.2020.110088
4. A. Trunschke, D.L. Hoang, H. Lieske, In situ FTIR studies of high-temperature adsorption of hydrogen on zirconia, J. Chem. Soc. Faraday Trans. 91 (1995) 4441-4444. https://doi.org/10.1039/ft9959104441
5. Harish Singh, Sunaina, Krishna Kumar Yadav, Vaibhav Kumar Bajpai, Menaka Jha, Tuning the bandgap of m-ZrO2 by incorporation of copper nanoparticles into visible region for the treatment of organic pollutants, Materials Research Bulletin, Volume 123, 2020, 110698. https://doi.org/10.1016/j.materresbull.2019.110698
6. T. Lopez, M. Alvarez, R. Gomez, D.H. Aguilar, P. Quintana,

ZrO2 and Cu/ZrO2 Sol-Gel Materials Spectroscopic Characterization, J. Sol-Gel Sci. Technol. 33 (2005) 93-97. https://doi.org/10.1007/s10971-005-6706-y
7. Y.H. Wang, W.G. Gao, H. Wang, Y.E. Zheng, W. Na, K.Z. Li, Structure-activity relationships of Cu-ZrO2 catalysts for CO2 hydrogenation to methanol: interaction effects and reaction mechanism, RSC Adv. 7 (2017) 8709-8717. https://doi.org/10.1039/C6RA28305E
8. T. Tsoncheva, I. Genova, M. Dimitrov, E. Sarcadi-Priboczki, A.M. Venezia, D. Kovacheva, N. Scotti, V. dal Santo, Nanostructured copper-zirconia composites as catalysts for methanol decomposition, Appl. Catal. B Environ. 165 (2015) 599-610. https://doi.org/10.1016/j.apcatb.2014.10.058
9. H. Zhuang, S. Bai, X. Lio, Z. Yan, Structure and performance of Cu/ZrO2 catalyst For the synthesis of methanol from CO2 hydrogenation, J. Fuel Chem. Technol. 38 (2010) 462-467. https://doi.org/10.1016/S1872-5813(10)60041-2
10. A. Fathy, O. Elkady, A. Abu-Oqail, Synthesis and characterization of Cu-ZrO2 nanocomposite produced by thermochemical process, J. Alloys Compd. 719 (2017) 411-419. https://doi.org/10.1016/j.jallcom.2017.05.209
11. S.V.H.S. Bhaskaruni, S. Maddila, W.E. van Zyl, S.B. Jonnalagadda, V2O5/ZrO2 as an efficient reusable catalyst for the facile, green, one-pot synthesis of novel functionalized dihydropyridine derivatives, Catal. Today. 309 (2018) 276-281. https://doi.org/10.1016/j.cattod.2017.05.038
12. L. Hu, H. Hu, W. Lu, Y. Lu, S. Wang, Novel composite BiFeO3/ZrO2 and its high photocatalytic performance under white LED visible-light irradiation, Mater. Res. Bull. 120 (2019) 110605. doi:10.1016/j.materresbull.2019.110605. https://doi.org/10.1016/j.materresbull.2019.110605
13. P. Joshi, S. Chakraborti, P. Chakrabarti, D. Haranath, V. Shanker, Z. A. Ansari, S. P. Singh, and V. Gupta, J. Nanosci. Nanotechnol. 9, 6427 (2009). https://doi.org/10.1166/jnn.2009.1584
14. D. De, S. M. Mandal, S. S. Gauri, R. Bhattacharya, S. Ram, and S. K. Roy, J. Biomed. Nanotechnol. 6, 138 (2010).
15. Sant Lal Jangra, K. Stalin, Neeraj Dilbaghi, Sandeep Kumar, Jai Tawale, Surinder P. Singh and Renu Pasricha, Antimicrobial Activity of Zirconia (Zr02) Nanoparticles and Zirconium Complexes, Journal of Nanoscience and Nanotechnology Vol. 12, 7 105- 7 112, 2012. https://iopscience.iop.org/article/10.1088/1742-6596/2114/1/012058/pdf
16. Jeba, R, Radhika, S, Padma,CM & Ascar Davix, X, 2021, 'Structural, Optical, Thermal, Magnetic Properties of Zirconia Nanorods and their Photocatalytic and Antimicrobial Properties', Journal of Water and Environmental Nanotechnology, 6(3):252-264. https://doi.org/10.22090/jwent.2021.03.006
17. Jeba, R, Radhika, S, Padma,CM & Ascar Davix, X, 2022, 'Antimicrobial and photocatalytic activities of strontium doped zirconium oxide nanoparticles', Materials Letters, vol. 311,no. 131559. https://doi.org/10.1016/j.matlet.2021.131559
18. Jeba, R, Radhika, S, Padma,CM & Ascar Davix X, 2022, 'Synthesis and characterization of zirconia nanorods as a photo catalyst for the degradation of methylene blue dye', Nanosystems: Physics, Chemistry, Maths, vol.13 (1), pp.78-86. https://doi.org/10.17586/2220-8054-2022-13-1-78-86
19. Jeba, R, Radhika, S, Padma,CM & Ascar Davix, X, 2022, 'Strontium doped zirconia for enhanced anti-microbial activity', Materials Today: Proceedings,vol.58,pp.927-931. https://doi.org/10.1016/j.matpr.2021.12.226
20. Abdullah Goktas, Sait Modanlı, Ahmet Tumbul, Ahmet Kilic, 2022, 'Facile synthesis and characterization of ZnO, ZnO:Co, and ZnO/ZnO:Co nano rod-like homojunction thin films: Role of crystallite/grain size and microstrain in photocatalytic performance', Journal of Alloys and Compounds, Volume 893. no. 162334. https://doi.org/10.1016/j.jallcom.2021.162334
21. T El-Achkar and D Weygand 2019 Modelling Simul. Mater. Sci. Eng. 27 055004. https://doi.org/10.1088/1361-651X/ab1b7c